Fortgeschrittenen Praktikum II

Optical pumping

11.04.2016

Benjamin Winkelmann
Peter Spalthoff

Tutor: Dominik Schomas

Contents

List of Figures

1 Goal of the experiment

In this experiment, the process of optical pumping will be used to precisely measure properties of Rubidium atoms such as the hyperfine constant A via absorption measurements. In addition to that, relaxation times of the induced pumped states as well as external magnetic fields will also be measured by observing the effect of magnetic fields, applied through Helmholtz coils, high frequency radio waves and variations in the laser intensity.

2 Physical principles

2.1 Hyperfine structure and Zeeman splitting

This section is based on the detailed elaborations in [1].
The fine structure levels of the atomic spectrum, which splits the basic levels into sublevels due to spin-orbit interaction, can be shown to be split into even finer levels, whose energetic distances are roughly three orders of magnitude smaller than those of the fine structure. This is called the 'hyperfine structure' and is mainly caused by the interaction of the nuclear magnetic dipole and quadrupole moment and the magnetic field of the shell electrons. Its structure for the two Rubidium isotopes that are used in this experiment can be seen in figure 2.1.

As the nucleus is charged and, expressed as the nuclear spin $\vec{I}$, has angular momentum, it also has a magnetic moment, which is $\vec{\mu}_I = \frac{g_I \mu_K}{\hbar} \vec{I}$, where g_I is the g-factor of the nucleus and μ_K is the nuclear magneton.
With the total angular momentum of the electrons $\vec{J}$, the total angular momentum of the atom can be written as

$$\vec{F} = \vec{J} + \vec{I}, \qquad |I - J| \leq F \leq I + J \tag{2.1}$$

The energy difference between hyperfine structure levels can then shown to be

$$\Delta E_{HFS} = -\vec{\mu}_I \cdot \vec{B}_J = \frac{A}{2}(F(F+1) - J(F+1) - I(I+1)) \tag{2.2}$$

where $A = \frac{g_I \mu_K B_J}{\sqrt{J(J+1)}}$ is the hyperfine constant. Neighboring levels thus have an energy difference of

$$\Delta E_{HFS}(F+1) - \Delta E_{HFS}(F) = A(F+1) \tag{2.3}$$

This structure for the rubidium isotopes used in this experiment can be seen in figure 2.2.

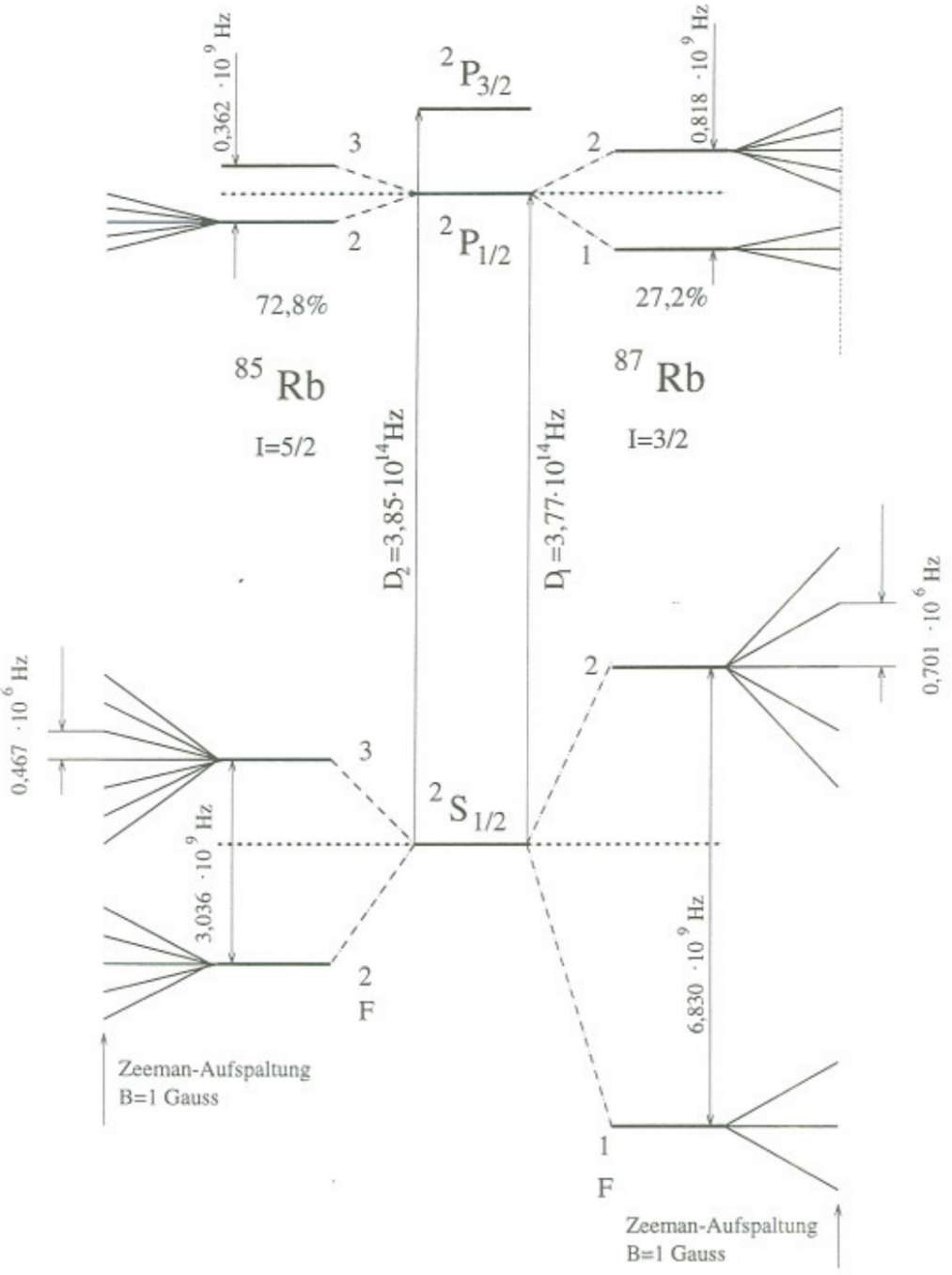

Figure 2.1: The hyperfine structure of the two isotopes of Rubidium used in the experiment. The hyperfine levels in turn are split due to the Zeeman effect caused by an external field of $B = 1$ G. [1]

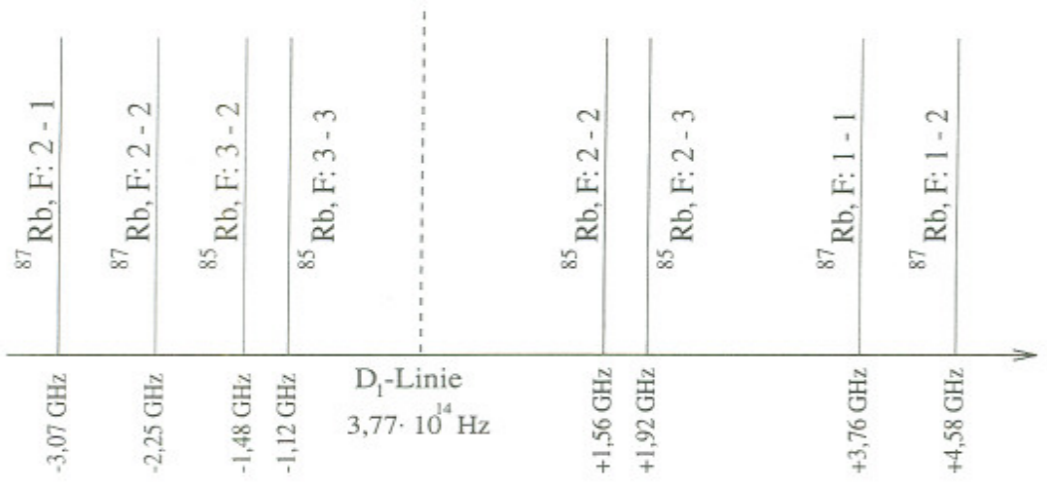

Figure 2.2: Energies of a set of hyperfine levels of the two isotopes used in the experiment. [1]

These hyperfine levels can in turn be split into $2(F+1)$ sub-levels in the presence of an external magnetic field. The according quantum number is $-F \leq m_F \leq F$. As long as the magnetic field is weaker than the spin-orbit coupling or, in other terms, $g_J \mu_B B_0 \ll A$, this is called the Zeeman effect. The effect for larger fields, where the spin-orbit coupling is disrupted, is called Paschen-Back effect.
For the Zeeman effect, the energy difference of the levels is

$$\Delta E_{Zeeman} = \frac{g_J}{2(I+\frac{1}{2})} \mu_B B_0 \tag{2.4}$$

where μ_B is the Bohr magneton.

2.2 Optical pumping

In general, pumping refers to constantly transferring electrons into higher energy levels until significantly more electrons are in the higher than in the lower state. This is called population inversion.
In the case of this experiment, this is done using a laser diode. As the goal is to examine magnetic fields using the Zeeman splitting, a way must be found to create population inversion within a single non-degenerate hyperfine structure level. Normally, electrons are equally distributed between said levels.
The selection rules for transitions

$$\begin{aligned} \Delta F &= 0, \pm 1 \qquad (F = 0 \nleftrightarrow F = 0) \\ \Delta m_F &= 0, \pm 1 \end{aligned} \tag{2.5}$$

allow for a convenient way to change that. If only σ^+-polarized light is used, only transitions with $\Delta m_F = +1$ are caused. Since the following decay is random within the

bounds of the transition rules, the laser will pump all electrons into the $^2S_{1/2}$ state with $m_F = +2$, $F = 2$ for ^{87}Rb and $m_F = +3$, $F = 3$ for ^{85}Rb. Figure 2.3 illustrates this for two exemplary transitions.
Mathematically, this process can be described as

$$\left(\frac{dn}{dt}\right)_P = \frac{N-n}{T_P} \tag{2.6}$$

where n is difference of the levels in the two-level system, N the overall number of atoms in the system and T_P the characteristic pumping time of the system.

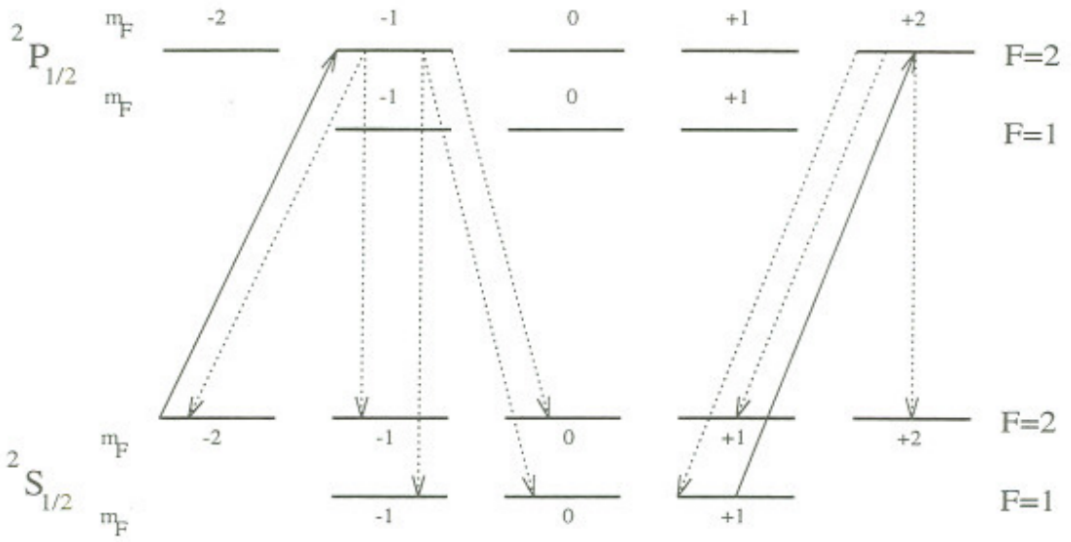

Figure 2.3: Optical pumping for ^{87}Rb. The σ^+ polarized light can only cause transitions with $\Delta m_F = +1$, thus achieving the desired pumping effect.

2.3 Relaxation processes

The desired pumping effect is counteracted mainly by three relaxation effects:

Diffusion to the wall: Upon hitting the glass containment, the rubidium atoms may lose their polarization. This process is inhibited by a buffer gas, which limits the mean free path of the atoms.

Collisions with the buffer gas: The rubidium atoms may use their polarization due to collisions with the buffer gas. The cross section of this event depend highly on what kind of gas is used. Best results are achieved with noble gases - in the case of this experiment, krypton was used.

Spin exchange When rubidium atoms collide, they may interchange their spins. While the overall polarization is preserved, the decoupling of nuclear and electron spins lead to a faster relaxation time. Much more detailed elaborations can be found in [3].

Overall, the relaxation can be described by the following differential equation

$$\left(\frac{dn}{dt}\right)_R = -\frac{n}{T_R} \tag{2.7}$$

where T_R is the characteristic relaxation time. A value of $T_R^{theo} = [\,6.5]ms$ is given in [1]. The overall process of polarization orientation is thus the sum of equations 2.6 and 2.7:

$$\left(\frac{dn}{dt}\right)_O = \left(\frac{dn}{dt}\right)_P + \left(\frac{dn}{dt}\right)_R = \frac{N}{T_P} - n\left(\frac{1}{T_P} + \frac{1}{T_R}\right) \tag{2.8}$$

The solution of this equation is an exponential

$$n(t) \propto e^{-\frac{t}{\tau}} \tag{2.9}$$

where $\tau = \frac{1}{T_P} + \frac{1}{T_R}$.

2.4 Larmor precession of the spin

If the ensemble is polarized along a certain magnetic field and one component of said field is suddenly set to zero, the polarization precesses around the remaining field. The precession frequency is

$$f_L = \frac{g_F \mu_B}{h} \cdot B =: \alpha \cdot B \tag{2.10}$$

where g_F are the Landé factors for the rubidium isotopes, quantified by Baur [1] as $g_F(^{85}Rb) = 1/3$ and $g_F(^{87}Rb) = 1/2$. The proportionality constant between the frequency and the remaining magnetic field thus is

$$\alpha(^{85}Rb) = 4.665\,\mathrm{kHz}/\mu\mathrm{T} \quad \alpha(^{87}Rb) = 6.998\,\mathrm{kHz}/\mu\mathrm{T} \tag{2.11}$$

3 Double resonance

3.1 Set-up and procedure

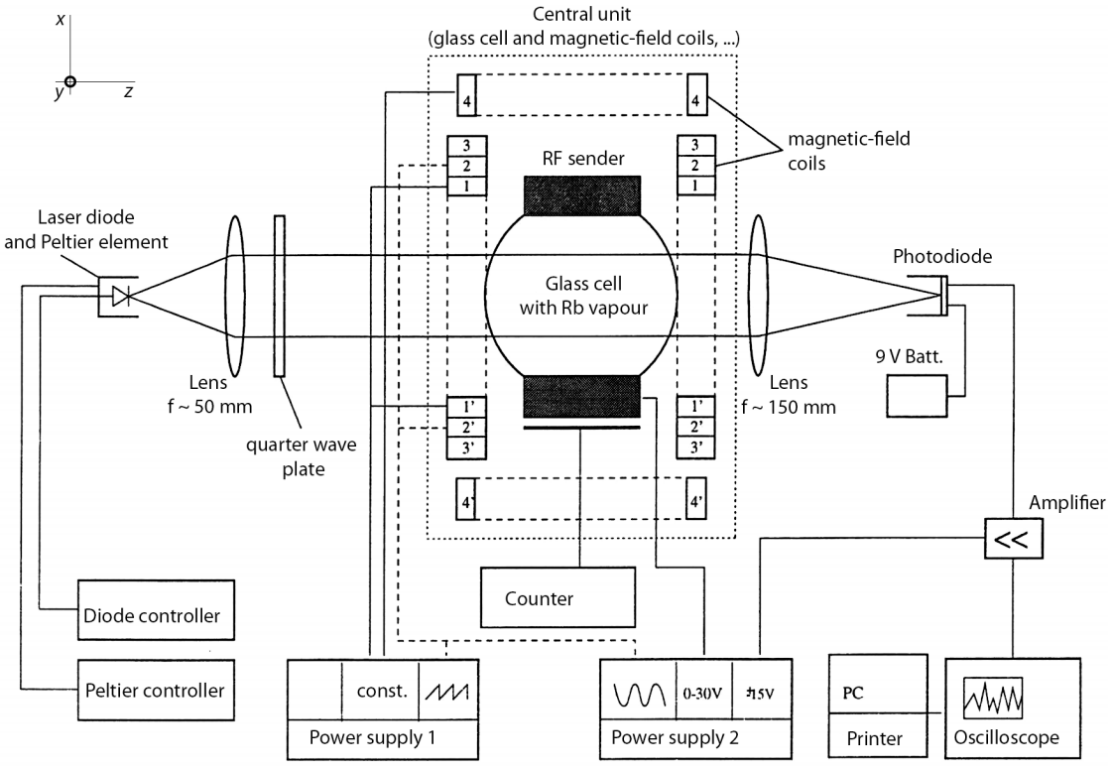

Figure 3.1: Experimental set-up for the double resonance measurements.[2]

This measurement is called double resonance since we both pump the Zeeman states and, at the same time, depopulate the polarized state with radio frequency radiation (RF radiation from here on). Both effects can be described as a resonance. The RF frequency can be measured with a frequency counter which is also built into the glass cell unit. The glass cell is now always lodged in the central unit.
To achieve pumping, the polarization of the laser light needs to be changed from linear to circular. It does not matter where it is right or left circular - that merely changes the direction of polarization. To achieve circular polarization, a quarter wave plate is used. As the polarization after said place depends on the angle of the linear polarization of the incident light, one has to check whether the light is actually circularly polarized after the wave plate. For that, a linear polarizer is used to check whether or not the intensity signal varies upon turning the linear polarizer, which it should not.
A sinusoid current is run through coil 2 (see fig. 3.1), at first with a large amplitude to find the magnetic field range for which double resonance occurs. Once the range is determined, a constant current is applied to coil 1. The double resonance peaks are now visible, but Dehmelt peaks, which are a result of relaxation once the magnetic field

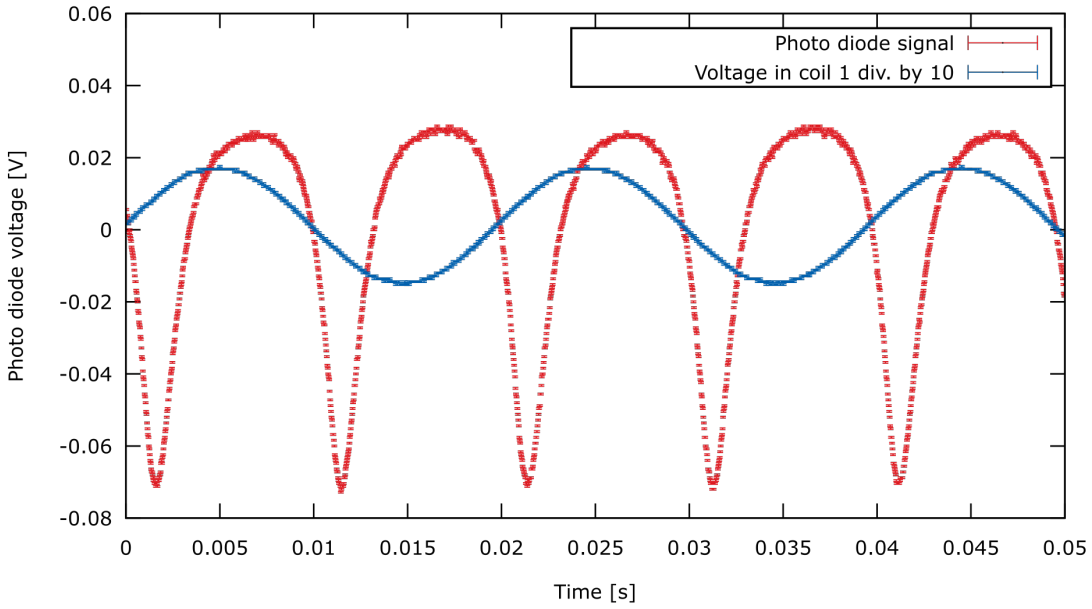

Figure 3.2: Equidistant peaks for $I_L = 61.8\,\text{mA}$ and a current in coil 1 of $I_{C1} = 130.2\,\text{mA}$. Note the phase shift: The double resonance peaks do not occur at the zero-crossing of the coil voltage, but at those of the coil current. The coil voltage was divided by ten to make the photo diode signal more dominant.

crosses zero, are still visible. It can easily be determined which is which, as the double resonance peaks disappear when one turns off the RF generator. For the Dehmelt peaks to disappear, the amplitude of the sinusoid in current two has to be reduced so that the overall magnetic field does not cross zero anymore. Coil 4, which creates a field along the x-axis in figure 3.1, can now be used to compensate the vertical magnetic field of the earth. When it is compensated, the negative peaks should have maximal depths. The current through coil 4 is then kept at this value for the main measurement.
With the vertical magnetic field compensated, the current in coil 1 can now be tuned to make the two peaks per period equidistant. In this state, the magnetic field from coil 1 stretches the Zeeman spectrum exactly enough for the RF frequency to relax the polarization. One such value must exist for both current directions through coil 1. This is done for both rubidium isotopes. The laser current is measured with an exterior multimeter, since the digital display is on has a precision of 1 mA. From these four values, the longitudinal magnetic field of the earth can be measured and the nuclear spins I of th isotopes calculated.

Coil No	n	d [m]	calc. B/I $[\frac{\text{Vs}}{\text{Am}^2}]$	meas. B/I $[\frac{\text{Vs}}{\text{Am}^2}]$
1	80	0.09	$8.0 \cdot 10^{-4}$	$7.99(1) \cdot 10^{-4}$
2	80	0.09	$8.0 \cdot 10^{-4}$	$8.14(1) \cdot 10^{-4}$
3	16	0.09	$1.7 \cdot 10^{-4}$	–
4	60	0.246	$4.4 \cdot 10^{-4}$	$4.76(1) \cdot 10^{-4}$

Table 3.1: The B/I values and properties of the Helmholtz coils. n is the number of windings. [2]

I_L [mA]	s_{I_L} [mA]	I_{C1} [mA]	$s_{I_{C1}}$ [mA]	B_{C1} [µT]	$s_{B_{C1}}$ [µT]
62.4	0.1	91.2	0.5	71	10
62.4	0.1	-85.3	0.5	85	9
61.8	0.1	136.1	0.5	109	12
61.8	0.1	-130.2	0.5	104	11

Table 3.2: The results of the double resonance measurements. The magnetic field signs were matched with those of the currents.

3.2 Data analysis

Measurements were taken at $T = 34.4°$ and with a RF frequency of $\nu_{RF} = (497 \pm 1) \cdot 10^3$ Hz. An uncertainty of $s_{I_{C1}} = 0.5$ mA was estimated for current at which the peaks are equidistant. The results can be seen in table 3.2. The current in coil 4 for which the vertical field was compensated was determined to be $I_{C4} = (78 \pm 3)$ mA.
The constants $c_B = B/I$ of the coils in table 3.1 were provided for the calculations of the magnetic fields that the coils create.
The magnetic fields are

$$B = c_b \cdot I_C, \qquad s_B = \sqrt{(c_b \cdot s_{I_C})^2 + (I_C \cdot s_{c_b})^2} \tag{3.1}$$

where I_C is the current in the respective coil. Table 3.2 lists those results for coil 1. From the current in coil 4, the vertical magnetic field was calculated to be

$$B_v = (37.1 \pm 1.4)\ \mu\text{T} \tag{3.2}$$

The magnetic fields are all written with positive sign. Let B_1 be the magnetic field of the positive, B_1' the negative coil current. The horizontal component of the earths' magnetic field is equal to half the difference of these two fields

$$B_h = \frac{B_1 - B_1'}{2}, \qquad s_{B_h} = \frac{1}{2} \cdot \sqrt{s_{B_1}^2 + s_{B_1'}^2} \tag{3.3}$$

The magnetic field difference is identical for the two isotopes, but the error is slightly different. The mean of the two is

$$B_h = (2.36 \pm 0.21)\ \mu\text{T} \tag{3.4}$$

When calculating the mean value of B_1 and B_1',

$$\overline{B}_1 = \frac{B_1 + B_1'}{2} \tag{3.5}$$

the magnetic field component of the earth cancels out and yields the magnetic field that is responsible for the Zeeman splitting. Together with the frequency ν_{RF} and by using equation 2.4, the nuclear spins I of the two isotopes can be calculated as

$$I = \frac{\mu_B \cdot \overline{B}_1}{h \cdot \nu} - \frac{1}{2}, \qquad s_I = \frac{\mu_B \cdot \overline{B}_1}{h \cdot \mu} \sqrt{\left(\frac{s_{\overline{B}_1}}{\overline{B}_1}\right)^2 + \left(\frac{s_\nu}{\nu}\right)^2} \tag{3.6}$$

Since greater diode current corresponds to lower frequency and thus lower transition energy, the current $I_{C1} = 62.4(1)$ mA corresponds to ^{87}Rb and the $I_{C1} = 61.8(1)$ mA to ^{85}Rb. The results for the spins were

$$I(^{85}\text{Rb}) = 2.496 \pm 0.009 \tag{3.7}$$

$$I(^{87}\text{Rb}) = 1.486 \pm 0.007 \tag{3.8}$$

$$\tag{3.9}$$

3.3 Discussion

The literature values for the earths' magnetic field are [2]

$$B_v^{lit} = 42.9\ \mu\text{T}, \quad B_h^{lit} = 20.9\ \mu\text{T} \tag{3.10}$$

while the measurements yielded $B_h = (2.36 \pm 0.21)\ \mu$T and $B_v = (37.1 \pm 1.4)\ \mu$T. While the result for the vertical field encloses the literature value in its 4σ interval, the result for the horizontal field is nowhere near the expected value. To double check the results, a Hall effect sensor was used. Since the sensor only had a resolution of 10 µT, it only useful for qualitative analysis. These measurements revealed that not only is the horizontal field much weaker inside the metal casing of the experimental set-up, the experimental set-up is also not aligned with the projection of the magnetic field lines on its horizontal axis. Due to time constraints, the measurements could not be repeated with an aligned table. The deviation in the vertical field can likely be attributed to shielding effects of the building.

The calculated values for the spins are in good agreement, enclosing the expected values of $I(^{87}) = 3/2$ in the 2σ interval and $I(^{85}) = 5/2$ in the 1σ interval.

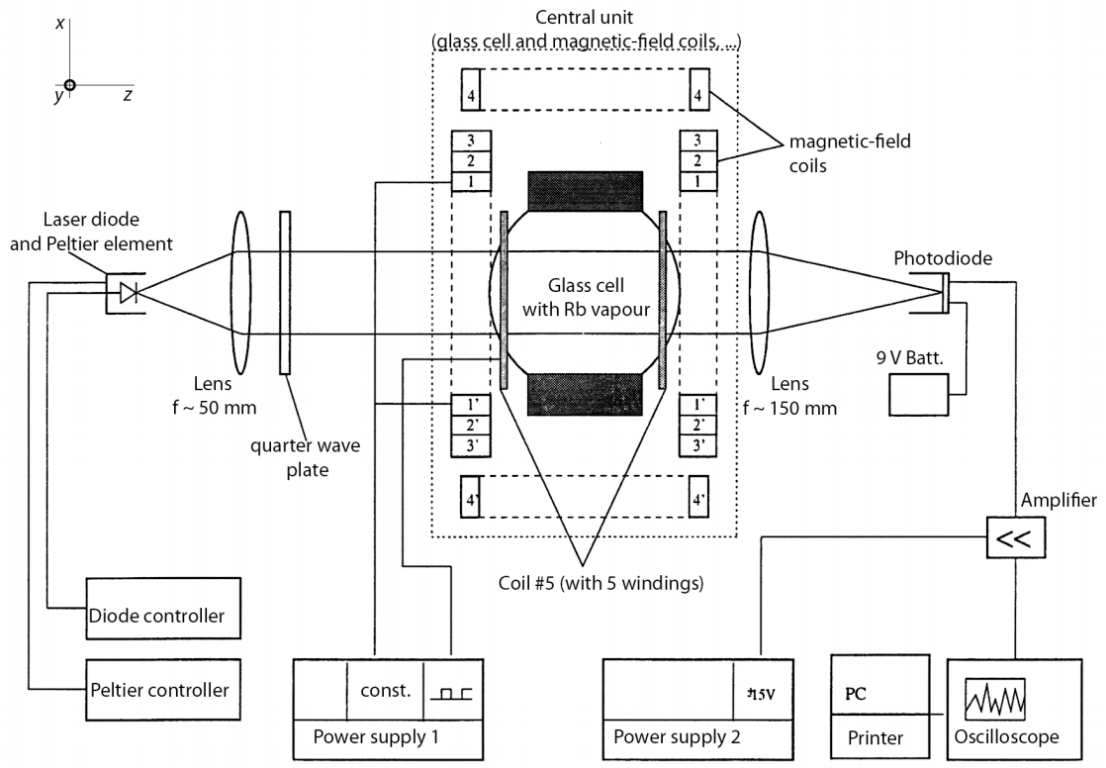

Figure 4.1: Experimental set-up for the spin precession measurements. [2]

4 Spin precession

4.1 Set-up and procedure

As before, only a quarter wave plate and the glass cell are placed in the beam. For the spin precession, the horizontal field as it was calculated in the double resonance section is compensated with a current in coil 1. A rectangular signal is given onto coil 5 so that the horizontal component of the magnetic field is compensated regularly. The spin precedes around the remaining vertical component, which can be varied by currents in coil 4. Measurements of the precession are then taken for a range of currents in coil 4.

Upon initial measurements, where both horizontal and vertical component were compensated as per the results from the double resonance section, it became clear that there was still a magnetic field, since precession could still be observed. As mentioned before, the table is not aligned with the horizontal component of the earths' magnetic field. Thus, the table was rotated until a minimal precession frequency was found. The degree by which the table was turned was by $\phi = (7 \pm 2)^\circ$ and measurements were then taken as described above.

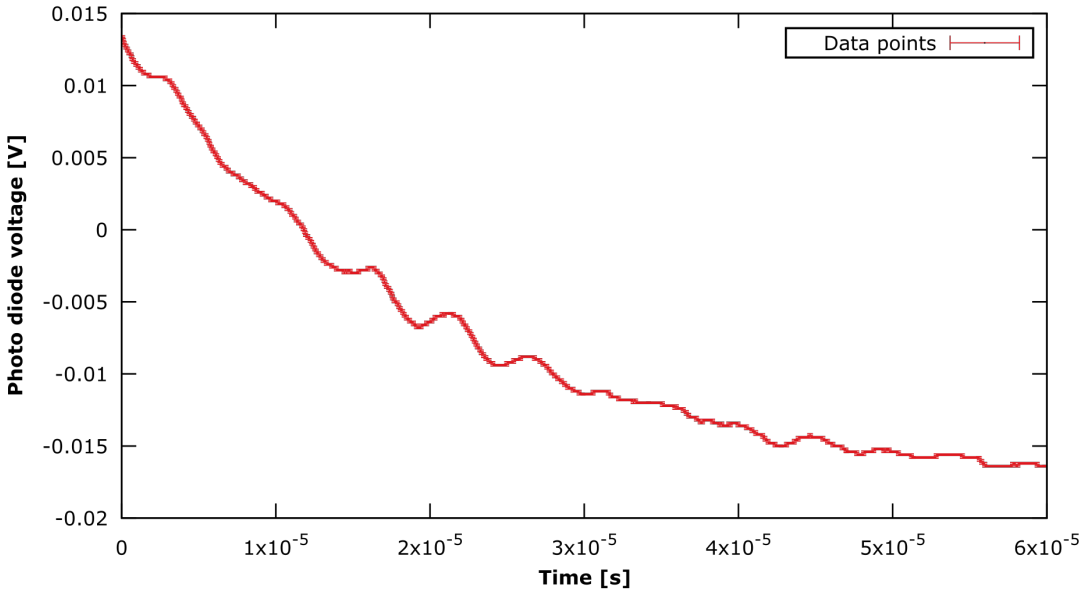

Figure 4.2: Examplary plot of the spin precession measurement. The peak positions were read off.

4.1.1 Analysis

Measurements were taken only for a diode current of $I_L = 62.0$ mA, which was the current corresponding to ^{87}Rb. No precession signal was found for ^{85}Rb. The temperature during the measurements was $T = 34.3°$ and the current for the compensation of the horizontal field after turning the table was $I_{C1} = (6 \pm 1)$ mA.
The time differences between peaks were read out of appropriate sub plots of the recorded data. One exemplary plot can be seen in figure 4.2 and all the values that were read out in table 4.1. First, the time difference Δt and its error were calculated

$$\Delta t = t_2 - t_1, \qquad s_{\Delta t} = \sqrt{2} \cdot s_{t_{12}} \tag{4.1}$$

where $s_{t_{12}}$ is the estimated error on reading the peaks as it is listed in table 4.1.
There sometimes were no properly readable adjacent peaks. While it was always clear that there was a peak, it was much easier to read out the second most adjacent peak. Those values are marked with a star in the first column in table 4.1 and their time difference is

$$\Delta t = \frac{t_2 - t_1}{2}, \qquad s_{\Delta t} = \frac{1}{\sqrt{2}} s_{t_{12}} \tag{4.2}$$

The precession frequency ν_L can now be calculated

$$\nu_L = \frac{1}{\Delta t}, \qquad s_{\nu_L} = \frac{s_{\Delta t}}{(\Delta t)^2} \tag{4.3}$$

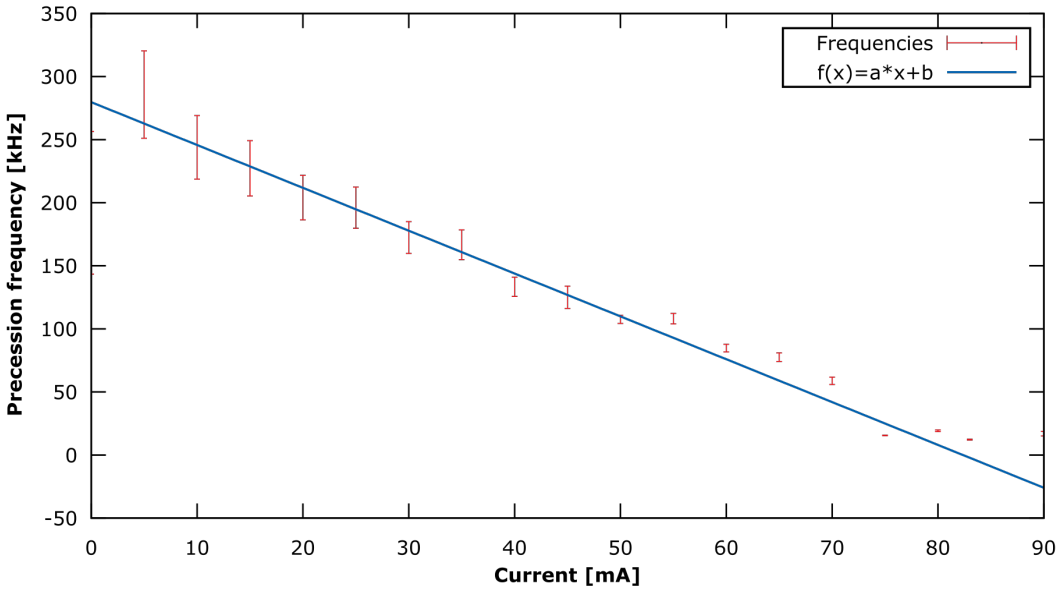

Figure 4.3: The precession frequencies and the according linear fit. The x-axis cut can be calculated from the fit parameters and represents the current in coil 4 for which the vertical magnetic field is fully compensated.

and the results are plotted in figure 4.3. A linear fit $f(x) = a \cdot x + b$ was used to describe the data and the resulting parameters were $a = (-3.40 \pm 0.17)$ kHz/mA and $b = (280 \pm 11)$ kHz with $\chi^2 = 9.9$. One can extrapolate to the magnetic field for which the precession frequency would be zero, assuming that all other fields were actually compensated for. The current in coil 4 for said field is $I^0_{C4} = \frac{-b}{a} = (82 \pm 5)$ mA and the according magnetic field $B_v = 39.2 \pm 2.5$ µT. This is within 1σ of the value calculated in the double resonance section.
Since the magnetic field is reduced until it reaches above field, the negative value of the fit constant a corresponds to the proportionality constant $\alpha_{lit} = 6.998$ kHz/µT between the magnetic field and the precession frequency as it was defined in 2.10. It is however still given in kHz/mA and needs to be translated to kHz/µT to be comparable. The result is

$$\alpha = \frac{a}{c_b}(7.1 \pm 0.4) \text{ kHz/µT} \tag{4.4}$$

where $c_b = 0.476(1)$ µT/mA is the proportionality factor between current and magnetic field for coil 4. This value includes the literature value in its 1σ interval.

I_{C4} [mA]	t_1 [10^{-5}s]	t_1 [10^{-5}s]	$s_{t_{12}}$ [10^{-5}s]
0	2.0	2.5	0.1
5	1.85	2.20	0.03
10	2.01	2.42	0.03
15	1.74	2.18	0.03
20	1.93	2.42	0.03
25	2.12	2.63	0.03
30	1.80	2.38	0.03
35	2.08	2.68	0.03
40	4.25	5.00	0.03
45*	4.52	5.32	0.04
50*	5.37	7.23	0.04
55*	5.38	7.23	0.05
60*	4.74	7.10	0.06
65*	5.45	8.03	0.08
70*	14.4	17.8	0.12
75	16.5	29.4	0.12
80	15.0	20.2	0.13
83	19.6	27.8	0.18
90	21.9	27.8	0.45

Table 4.1: The B/I values and properties of the Helmholtz coils. n is the number of windings. [2]

5 References

[1] Baur, Clemens. *Einrichtung des Versuchs "Optisches Pumpen mit Laserdioden".* Zulassungsarbeit. Freiburg 1997

[2] *Instructions for the experiment "Optical Pumping".* Albert-Ludwig University Freiburg. Freiburg 02.2016

[3] Happer, William. *Optical pumping.* Reviews of Modern Physics 44.2 (Apr. 1972): 170-238

[4] Corney, A. *Atomic and Laser Spectroscopy.* Oxford University Press, 1977